Comparative Analysis of Fixed-Parameter and UKF-Based Adaptive M^{2}PC-Controlled Induction Machines Under Parameter Variations

Ugur Ufuk Korpe
Dept. of Electrical-Electronics Engineering
Kirsehir Ahi Evran University
Kirsehir, Turkey
ugur.korpe@ahievran.edu.tr

Mustafa Gokdag
Dept. of Electrical-Electronics Eng.
Industrial Electronics Lab. (KBU-IEL)
Karabuk University
Karabuk, Turkey
mgokdag@karabuk.edu.tr

Ozan Gulbudak
Dept. of Electrical-Electronics Eng.
Industrial Electronics Lab. (KBU-IEL)
Karabuk University
Karabuk, Turkey
ozangulbudak@karabuk.edu.tr

2025 7th Global Power, Energy and Communication Conference (GPECOM) | 979-8-3315-1323-8/25/$31.00 ©2025 IEEE | DOI: 10.1109/GPECOM65896.2025.11061925

***Abstract*— This paper presents a simulation-based comparative analysis of Modulated Model Predictive Control (M^{2}PC) strategies under parameter variations in induction motors. Two control schemes are evaluated: one using fixed (nominal) parameters and another integrating an Unscented Kalman Filter (UKF) for online estimation of magnetizing inductance (L_m) and rotor resistance (R_r). Results have shown that parameter mismatch significantly affects electromagnetic torque production, flux regulation, and power quality, leading to performance degradation. The UKF-based controller effectively compensates for these deviations, maintaining accurate torque and flux control. These findings are particularly relevant for electric vehicle applications, where direct torque control is essential. In such systems, unaccounted parameter variations can lead to torque deficits and loss of drive accuracy. The study demonstrates that integrating UKF into model-based control enhances system robustness, efficiency, and torque delivery under dynamic conditions.**

Keywords—Induction machine, modulated model predictive control, torque production, Unscented Kalman filter, parameter estimation

I. INTRODUCTION

The foundations of high-performance speed and torque control systems for IMs were established with the introduction of Field Oriented Control (FOC) in 1972 and Direct Torque Control (DTC) in 1986 [1], [2]. Both techniques enabled decoupled control of the torque and flux-producing components of the machine [3]. However, these methods are based on linear control theory and were developed when microcontroller technology was not as widely available or advanced as today. Over the past three decades, microcontroller technology has experienced significant advancements. As a result, interest in nonlinear control strategies has grown considerably, particularly over the last 15 years. Among these nonlinear methods, Model Predictive Control (MPC) was initially adopted in the petrochemical industry due to the long sampling times, but its application in power electronics and machine control has expanded rapidly since the early 2000s, driven by the continuous development of microcontroller capabilities [4].

Model Predictive Control (MPC) is a general control framework that encompasses various control strategies. Among these, Finite Control Set Model Predictive Control (FCS-MPC) has gained particular popularity in the literature compared to other MPC approaches [5], [6]. FCS-MPC predicts system state variables for all possible control inputs using the system's discrete-time model. These predicted states are evaluated via a cost function, along with their references, to determine the optimal control action [7]. FCS-MPC has gained popularity in power electronics and electric machine control applications in recent years due to its ease of implementation, single-loop structure, and suitability for multivariable systems [8]–[10]. Additionally, it offers a fast dynamic response and enables direct incorporation of nonlinearities and system constraints (e.g., voltage and current limits) into the control design through the mathematical model [11], [12]. However, the absence of a modulator in FCS-MPC causes the same voltage vector to be applied over consecutive cycles, leading to variable switching frequency [13]. At low switching frequencies, this results in increased phase current total harmonic distortion (THD) and torque ripple, degrading steady-state performance [14]. Reducing the sampling period can address these issues but increases the computational burden. As an alternative, the M^{2}PC technique introduces a modulation block into FCS-MPC, selecting an optimal sector and corresponding duty cycles rather than a direct voltage vector [15], [16]. These duty cycles are then converted into switching signals via standard modulation methods. Recent studies confirm that M^{2}PC achieves fixed switching frequency, reduced THD, and improved torque quality without additional computational cost [17]–[19]. Both FCS-MPC and M^{2}PC rely on the discrete-time mathematical model of the machine's dq- axis currents, where the accuracy of machine parameters strongly influences the overall control performance [20], [21]. IM model includes significant electrical parameters such as stator and rotor resistances and inductances, and it exhibits strong cross-coupling characteristics. These parameters vary nonlinearly with temperature, magnetic saturation, skin effect, and the machine's operating region [22], [23]. Typically, resistances change in the constant torque region, whereas inductances vary in the constant power region. Neglecting these variations and using fixed nominal values in the control loop leads to inaccurate reference calculations, poor torque control, and reduced efficiency [24]. Therefore, integrating parameter estimation techniques into the control framework is essential for maintaining performance under varying conditions.

In the literature, several observer-based online parameter estimation methods have been applied to IMs, including MRAS, Kalman Filter (KF)-based techniques such as EKF and UKF, and observer designs like sliding mode observer (SMO) and Luenberger Observer [25]–[31]. MRAS-based studies primarily investigate the impact of rotor time constant on control performance [25], [26], with parameter estimation relying on mathematical models of physical quantities such as reactive and active power, making MRAS inherently model-dependent. Among KF-based methods, EKF is more widely adopted, focusing on estimating rotor speed and load torque and their influence on control performance [27], [29]–[31]. EKF extends classical KF to mildly nonlinear systems through recursive linearization via Jacobian matrices, but its reliance on first-order Taylor expansion can limit accuracy in highly

979-8-3315-1323-8/25/$31.00 ©2025 IEEE

nonlinear models [31]. To address this, Julier and Uhlmann [32] proposed the Unscented Transform (UT), which propagates sigma points through nonlinear dynamics to compute posterior statistics without explicit derivatives [33]. Based on this principle, UKF was introduced as a more robust and derivative-free alternative for nonlinear estimation [34]. Given the nonlinear nature of IMs, the UKF is selected in this study for accurate and adaptive parameter identification. Despite extensive studies, the direct impact of magnetizing inductance and rotor resistance variations on control performance has not been explicitly examined. Moreover, instead of adopting M²PC structures, prior works such as [25], [28], [29] have predominantly focused on Model Predictive Torque Control (MPTC) within the general MPC framework. To address this gap, this study compares the dynamic and steady-state responses of two M²PC-based controllers—one using fixed (nominal) parameters and the other integrating UKF for online estimation—under variations in L_m and R_r. The performance comparison highlights the adverse effects of parameter deviations, such as inaccurate dq-axis current and voltage tracking, reduced torque capability, increased reactive power, and decreased power factor. By estimating Lm and Rr with errors below 10%, the UKF-based approach mitigates these issues effectively. The paper is organized as follows: Section I reviews control and estimation strategies; Section II presents the control system model; Section III details the UKF formulation; and Section IV provides and discusses simulation results.

II. MATHEMATICAL MODEL OF THE CONTROL SYSTEM

A. Voltage-source inverter model

This section presents the mathematical formulation of the overall control system, which includes the voltage source inverter (VSI), IM, and M²PC structure. The system employs a three-phase two-level VSI as the power converter, whose topology is illustrated in Fig. 1. The inverter is assumed to be ideal and operates under balanced load conditions. The phase-to-neutral voltages corresponding to phases A, B, and C are defined in equation (1) [35].

$$\begin{bmatrix} V_{An} \\ V_{Bn} \\ V_{Cn} \end{bmatrix} = \frac{V_{DC}}{3} \begin{bmatrix} 2 & -1 & -1 \\ -1 & 2 & -1 \\ -1 & -1 & 2 \end{bmatrix} \begin{bmatrix} S_1 \\ S_3 \\ S_5 \end{bmatrix} \tag{1}$$

where switch position $S_j \in \{0,1\}$.

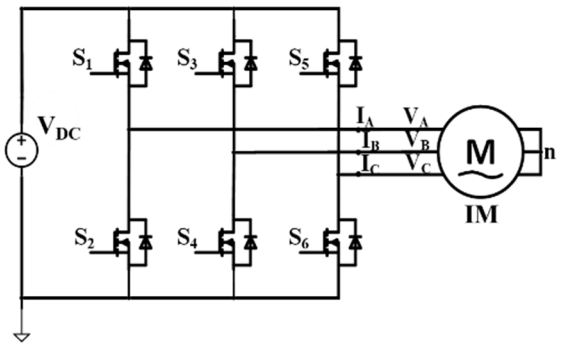

Fig. 1. A voltage-source inverter connected to IM

B. Dynamic model of IM and M²PC

The three-phase stator currents are transformed into dq-axis currents using the Park transformation, as shown in (2)-(3) [36].

$$\frac{di_{sd}}{dt} = -\frac{L_r R_s + L_m^2/\tau_r}{\sigma L_s L_r} i_{sd} + \omega_g i_{sq} + \frac{L_m}{\tau_r \sigma L_s L_r} \psi_{rd} + \frac{v_{sd}}{\sigma L_s} + \frac{L_m}{\sigma L_s L_r} \omega_e \psi_{rq} \tag{2}$$

$$\frac{di_{sq}}{dt} = -\frac{L_r R_s + L_m^2/\tau_r}{\sigma L_s L_r} i_{sq} - \omega_g i_{sd} + \frac{L_m}{\tau_r \sigma L_s L_r} \psi_{rq} + \frac{v_{sq}}{\sigma L_s} - \frac{L_m}{\sigma L_s L_r} \omega_e \psi_{rd} \tag{3}$$

where v_{sd}, v_{sq} are d-q axis stator voltages, i_{sd}, i_{sq} are dq- axis currets, ψ_{rd}, ψ_{rq} are d-q axis rotor fluxes, L_s, L_r, L_m are stator, rotor, and mutual inductances, respectively, $\tau_r = L_r/R_r$ is rotor time constant, $\sigma = (L_r L_s - L_m^2)/L_r L_s$ is leakage constant, ω_g is synchronous angular speed, $\omega_e = P\omega_m$ is electrical angular speed where P is the machine pole pair number, and ω_m is mechanical angular speed. Similarly, the three-phase rotor flux components are also transformed into the dq- reference frame using the same transformation, and are expressed in (4)-(5). The electromagnetic torque equation of the machine is given in (6).

$$\frac{d\psi_{rd}}{dt} = \frac{L_m}{\tau_r} i_{sd} - \frac{\psi_{rd}}{\tau_r} + (\omega_g - \omega_e)\psi_{rq} \tag{4}$$

$$\frac{d\psi_{rq}}{dt} = \frac{L_m}{\tau_r} i_{sq} - \frac{\psi_{rq}}{\tau_r} - (\omega_g - \omega_e)\psi_{rd} \tag{5}$$

$$T_e = \frac{3P}{2}\frac{L_m}{L_r}(\psi_{rd} i_{sq} - \psi_{rq} i_{sd}) \tag{6}$$

Rotor flux orientation is applied to the machine, which results in the q- axis rotor flux, ψ_{rq}, and its derivative, $d\psi_{rq}/dt$, being zero under the steady-state condition. Consequently, the slip value of the machine can be estimated as defined in (7) [36].

$$\omega_{sl} = \omega_g - \omega_e = \frac{L_m}{\tau_r \psi_{rd}} i_{sq} \tag{7}$$

With rotor flux orientation, the d- axis stator current becomes directly proportional to the d- axis rotor flux (i.e., reference flux), as given in (8). Moreover, since the q- axis rotor flux is 0, the electromagnetic torque equation in (6) simplifies to a more tractable form, as shown in equation (9) where $K_t = 3PL_m\psi_{rd}/2\,L_r$ is the torque constant, which allows torque control via the q- axis stator current.

$$i_{sd} = \frac{\psi_{rd}}{L_m} \tag{8}$$

$$T_e = K_t i_{sq} \tag{9}$$

To implement the M²PC technique, the continuous-time dq- axis stator current and rotor flux equations given in (2)–(5) are discretized using the Forward Euler Method (FEM). The resulting discrete-time formulations are presented in (10)–(13).

$$i_{sd}(k+1) = \left(1 - \frac{L_r R_s + L_m^2/\tau_r}{\sigma L_s L_r} T_s\right) i_{sd}(k) + T_s\left(\omega_g(k) i_{sq}(k) + \frac{L_m}{\tau_r \sigma L_s L_r} \psi_{rd}(k)\right) + T_s\left(\frac{v_{sd}(k)}{\sigma L_s} + \frac{L_m}{\sigma L_s L_r} \omega_e(k) \psi_{rq}(k)\right) \tag{10}$$

$$i_{sq}(k+1) = \left(1 - \frac{L_r R_s + L_m^2/\tau_r}{\sigma L_s L_r} T_s\right) i_{sq}(k) + T_s\left(-\omega_g(k) i_{sd}(k) + \frac{L_m}{\tau_r \sigma L_s L_r} \psi_{rq}(k)\right) - T_s\left(\frac{L_m}{\sigma L_s L_r} \omega_e(k) \psi_{rd}(k) - \frac{v_{sq}(k)}{\sigma L_s}\right) \tag{11}$$

$$\psi_{rd}(k) = \psi_{rd}(k-1)\left(1-\frac{T_s}{\tau_r}\right) + T_s\left(\frac{L_m}{\tau_r} i_{sd}(k-1) + \left(\omega_g(k-1) - \omega_e(k-1)\right)\psi_{rq}(k-1)\right) \quad (12)$$

$$\psi_{rq}(k) = \psi_{rq}(k-1)\left(1-\frac{T_s}{\tau_r}\right) + T_s\left(\frac{L_m}{\tau_r} i_{sq}(k-1) - \left(\omega_g(k-1) - \omega_e(k-1)\right)\psi_{rd}(k-1)\right) \quad (13)$$

The relationship between the rotor's electrical angle and machine's ω_g is expressed in (14). By applying the FEM with a one-step backward shift, the discrete-time form of the electrical angle is obtained, as shown in (15) [36].

$$\frac{d\theta_e}{dt} = \omega_g \quad (14)$$

$$\theta_e(k) = \theta_e(k-1) + T_s\omega_g(k-1) \quad (15)$$

where θ_e is the electrical angle of the machine. The block diagram of the designed control system is presented in Fig. 5. As illustrated in Fig. 5, the d-axis reference current is computed using (8). The q- axis reference current is obtained by dividing the electromagnetic torque generated by the outer loop controller by K_t, as given in (9). Using the measured dq-axis currents, machine parameters, and (1), the voltage vectors corresponding to the eight switching states are substituted into (10)-(11) to predict eight possible current values. Each predicted current is then evaluated using the cost function defined in (16), by comparing it with the corresponding reference value.

$$G = (I_{d,ref} - I_d(k+1))^2 + (I_{q,ref} - I_q(k+1))^2 \quad (16)$$

Unlike the conventional FCS-MPC approach, the switching vector associated with the minimum cost is not directly applied to the inverter. Instead, the sector corresponding to that vector is selected as the optimal sector. Subsequently, the duty cycles for the selected sector are computed using (17)–(19) [37].

$$d_0 = \frac{T_s(G_{d1}G_{q2} - G_{d2}G_{q1})}{D} \quad (17)$$

$$d_1 = \frac{T_s(G_{d2}G_{q0} - G_{d0}G_{q2})}{D} \quad (18)$$

$$d_2 = \frac{T_s(G_{d0}G_{q1} - G_{d1}G_{q0})}{D} \quad (19)$$

Here, d_j denotes the duty cycles of the active and zero vectors for j=0,1,2 and G_{dj}, G_{qj} represent the corresponding current errors. The variable D is defined in (20). In this study, Space Vector Pulse Width Modulation (SVPWM) is selected as the modulation technique. Accordingly, the calculated duty cycles are applied to the SVPWM block, which generates the corresponding switching signals to control the inverter.

$$D = G_{d0}G_{q1} - G_{d1}G_{q0} - G_{d0}G_{q2} + G_{d2}G_{q0} + G_{d1}G_{q2} - G_{d2}G_{q1} \quad (20)$$

III. UNSCENTED KALMAN FILTER

In order to implement the UKF, the discrete-time control system must be represented in a state-space form, as described in (21). In this study, a sixth-order model of the induction motor is employed, where the state vector x_k is defined based on the input vector $x = [i_{sd}(k), i_{sq}(k), \psi_{rd}(k), \psi_{rq}(k), L_m(k), R_r(k)]$ and includes both states and parameters to be estimated. y_k is the output matrix, which consists of $y = [i_{sd}, i_{sq}]$. It is assumed that the machine parameters L_m and R_r within the state vector x_k vary slowly over time. Therefore, their time derivatives dL_m/dt and dR_r/dt are considered to be 0.

$$\begin{aligned} x_{k+1} &= f(x_k, u_k) + w_k \\ &= A(x_k)x_k + Bu_k + w_k \\ y_k &= h(x_k) + v_k \\ &= Hx_k + v_k \end{aligned} \quad (21)$$

A. Mathematical model of UKF

The UT is a nonlinear mapping technique used for accurately propagating the mean and covariance of a random variable through a nonlinear function. In the context of the UKF, the UT enables the application of Kalman filtering principles to nonlinear systems by avoiding linearization and instead using a deterministic sampling approach. Let $x_k \in \mathbb{R}^n$ be a random variable with a known mean $\widehat{x_k}$ and covariance P_x, and let the nonlinear transformation be given by $y_k = f(x_k)$, as expressed in (21). To approximate the statistical properties of y_k, a set of 2n+1 sigma points is generated, forming the matrix χ. These points are computed using the square root of the state covariance matrix, typically obtained via Cholesky decomposition [31], and scaled according to a parameter γ defined in (22)-(23).

$$\gamma = \sqrt{n+\lambda} \quad (22)$$

$$\lambda = \alpha^2(n+\kappa) - n \quad (23)$$

where α, β, κ are tuning parameters that control the spread and weighting of the sigma points. The weights for the mean and covariance are assigned as in (24)-(26).

$$W_0^{(m)} = \lambda/(n+\lambda) \quad (24)$$

$$W_0^{(c)} = (\lambda/(n+\lambda)) + 1 - \alpha^2 + \beta \quad (25)$$

$$W_i^{(m)} = W_i^{(c)} = 1/\big(2(n+\lambda)\big), i = 1,..,2n \quad (26)$$

Using these definitions, the sigma point matrix is generated as in (27):

$$\chi_{k-1} = \left[\widehat{x_{k-1}} \quad \widehat{x_{k-1}} + \gamma\sqrt{P_x} \quad \widehat{x_{k-1}} - \gamma\sqrt{P_x}\right] \quad (27)$$

Each sigma point is then propagated through the nonlinear system model $f(\cdot)$ as given in (28) to predict the next state.

$$\chi_{k|k-1} = f(\chi_{k-1}, u_{k-1}) \quad (28)$$

The predicted state mean $\widehat{x_k}^-$ and covariance P_k^- are then calculated as weighted sums given in (29)-(30).

$$\widehat{x_k}^- = \sum_{i=0}^{2n} W_i^{(m)} \chi_{i,k|k-1} \quad (29)$$

$$P_k^- = \sum_{i=0}^{2n} W_i^{(c)} \big(\chi_{i,k|k-1} - \widehat{x_k}^-\big)\big(\chi_{i,k|k-1} - \widehat{x_k}^-\big)^T + Q \quad (30)$$

where Q is the process noise covariance matrix. These calculations (22)-(30) are performed in the prediction step. To perform the measurement update, the predicted sigma points are passed through the measurement function $h(\cdot)$ in (31) to obtain the prediction measurements.

$$Y_{i,k|k-1} = h(\chi_{i,k|k-1}) \quad (31)$$

The predicted measurement mean $\widehat{y_k}$ and innovation covariance $P_{\widehat{y_k}\widehat{y_k}}$ are then computed as given in (32)-(33).

$$\widehat{y_k} = \sum_{i=0}^{2n} W_i^{(m)} Y_{i,k|k-1} \quad (32)$$

$$P_{\widehat{y_k}\widehat{y_k}} = \sum_{i=0}^{2n} W_i^{(c)} \big(Y_{i,k|k-1} - \widehat{y_k}\big)\big(Y_{i,k|k-1} - \widehat{y_k}\big)^T + R \quad (33)$$

The cross-covariance between the state and measurement is calculated as in (34).

$$P_{\widehat{x_k}\widehat{y_k}} = \sum_{i=0}^{2n} W_i^{(c)} \left(\chi_{i,k|k-1} - \widehat{x_k}^-\right)\left(Y_{i,k|k-1} - \widehat{y_k}\right)^T \quad (34)$$

Using the innovation covariance and cross-covariance, the Kalman gain, updated state estimate, and updated covariance are obtained as (35)-(37) [31].

$$K_k = P_{\widehat{x_k}\widehat{y_k}}\left(P_{\widehat{y_k}\widehat{y_k}}\right)^{-1} \quad (35)$$

$$\widehat{x_k} = \widehat{x_k}^- + K_k(y_k - \widehat{y_k}^-) \quad (36)$$

$$P_k = P_k^- - K_k P_{\widehat{y_k}\widehat{y_k}} K_k^T \quad (37)$$

This process is repeated at each sampling interval to recursively estimate the machine states and parameters in real-time using the UKF.

IV. SIMULATION RESULTS

The simulations of both M²PC-based controllers—one using fixed machine parameters and the other incorporating the UKF, as shown in Fig. 5—are performed in the MATLAB/Simulink© simulation environment. The parameters of the simulated IM and the simulation configuration are listed in Table I. The total simulation time is set to t=35 s. The reference rotor speed is defined as ω_{ref}=1000 rpm (104.7198 rad/s), and the load torque is set to T_L=3 Nm. In the UKF-based controller, although the UKF is active from the beginning of the simulation, nominal machine parameters are used in the control algorithm until t=7.5 s. After this time, the estimated values of L_m and R_r obtained from the UKF are applied in the control loop. For both controllers, R_r and L_m at the IM are kept at their nominal values until t=10 s. After t=10 s, in order to emulate the effects of temperature rise, R_r is increased by 30% from its nominal value using a ramp function over a duration of 5 seconds. Subsequently, Lm is decreased by 30% from its nominal value to represent the onset of magnetic saturation, using a 5-second ramp function. The results obtained from this simulation scenario are illustrated in Fig. 2-4 and Fig. 6-7.

Table I. Simulation and machine parameters

Parameter	Description	Values
V_{DC}	DC bus voltage	300 V
P	Number of pole pairs	2
$T_{e,nom}$	Nominal torque	7.5 Nm
$\omega_{m,nom}$	Nominal rotor speed	1500 rpm
L_m	Nominal mutual inductance	442.3 mH
L_{ls}	Nominal stator leakage inductance	10.145 mH
L_{lr}	Nominal rotor leakage inductance	10.061 mH
R_s	Nominal stator resistance	3.919 Ω
R_r	Nominal rotor resistance	4.9618 Ω
T_s	Sampling time	100 µs
f_s	Switching frequency	10 kHz

As shown in Fig. 2, the UKF estimates L_m and R_r with high accuracy, achieving an error margin below 10% even under intentional parameter variations, such as temperature-induced resistance changes and flux saturation effects. This validates the effectiveness of the UKF in tracking time-varying parameters in real-time. Fig. 3 illustrates that in the fixed-parameter case, deviations between the electromagnetic torque produced by the controller and the actual machine torque occur during parameter shifts. These deviations lead to a mismatch in rotor flux generation and affect the tracking performance of the dq-axis stator currents and voltages as given in Fig. 4 and Fig. 6. The observed torque tracking error results in incorrect slip computation, causing the rotor flux orientation to diverge from the desired field-oriented direction. This misalignment reduces control accuracy, degrades the power factor, and increases reactive power, as shown in Fig. 7.

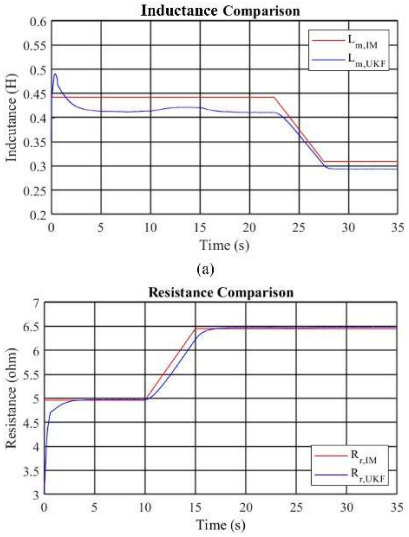

Fig. 2. UKF estimations: a) L_m, b) R_r

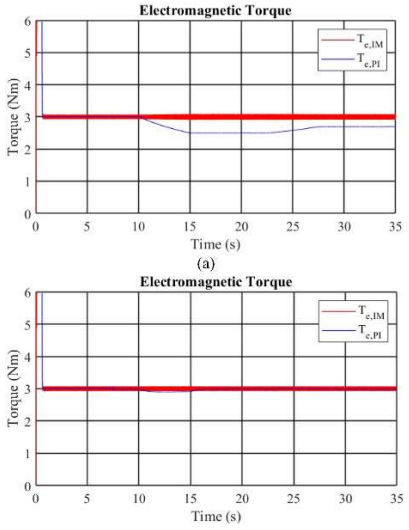

Fig. 3. Results of the designed control systems (Electromagnetic torque): a) Fixed parameter case, b) UKF case

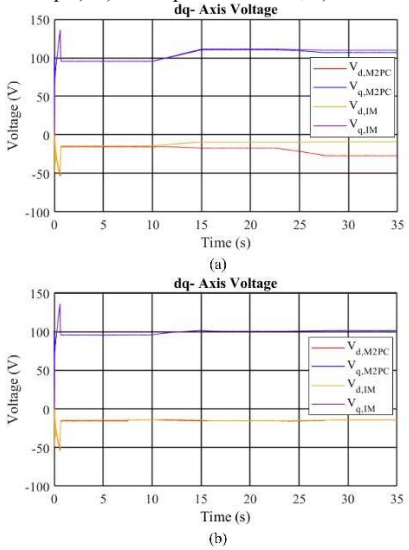

Fig. 4. Results of the designed control systems (dq- axis voltage): a) Fixed parameter case, b) UKF case

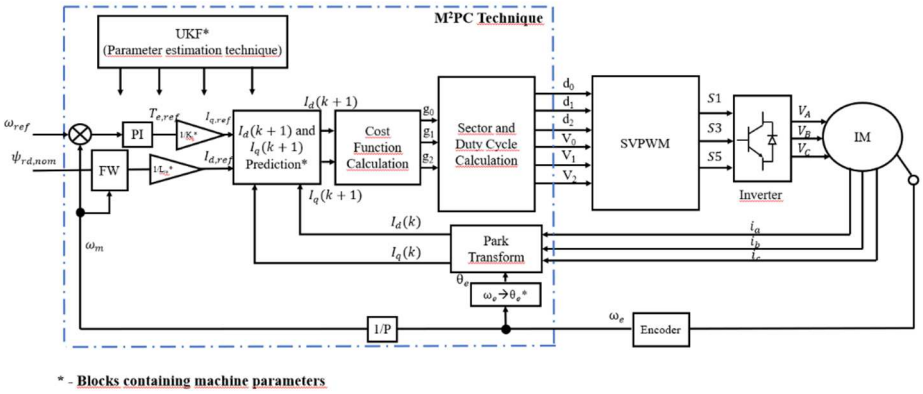

Fig. 5. Block diagram of the designed control systems

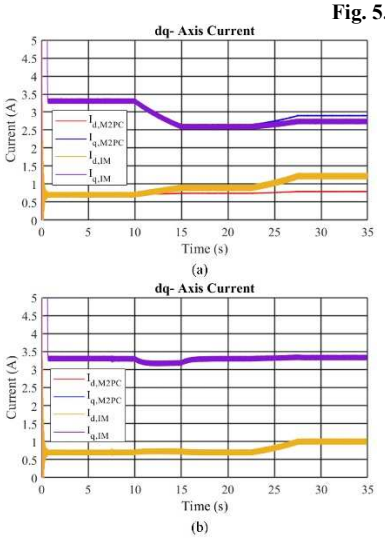

Fig. 6. Results of the designed control systems (dq- axis current): a) Fixed parameter case, b) UKF case

In contrast, the UKF-enhanced control system adapts to parameter variations effectively. As shown in Fig. 3(b), the controller maintains accurate torque tracking throughout the simulation. Fig. 4(b) and Fig. 6(b) confirm that the machine operates with improved flux alignment and maintains more accurate reference tracking for dq-axis currents and voltages. Moreover, Fig. 7 shows that the machine retains better field orientation and slip reference behavior under the UKF case. This contributes to more efficient operation and enhanced control robustness. From a power quality perspective, Fig. 7 highlights that the proposed UKF-based controller maintains a higher power factor (~0.91) and reduces reactive power generation by approximately 15 VAr compared to the fixed-parameter case. This improvement in tracking accuracy and power quality clearly demonstrates the robustness of the UKF-based controller under parameter variations. Such enhancements are particularly vital in electric vehicle applications, where torque control dominates during non-cruising modes. In the absence of real-time parameter estimation, mismatches between control models and physical machine behavior may lead to torque deficits, impairing drivability and efficiency. The proposed strategy ensures that the machine delivers the required torque accurately, even under varying operating conditions.

V. CONCLUSION

In this study, the impact of parameter variations on the performance of M²PC-based IM control was thoroughly investigated. A comparative analysis between fixed-parameter and UKF-supported adaptive controllers was performed using detailed simulation scenarios. The results show that fixed-parameter controllers suffer from poor torque and flux control, leading to inaccurate dq- axis reference tracking, decreased power factor, and increased reactive power. In contrast, the UKF-based controller dynamically estimates L_m and R_r with an error below 10%, enabling the system to maintain accurate torque production and field orientation under varying conditions. The adaptive controller also improves power quality by reducing reactive power and sustaining a higher power factor. These findings underscore the importance of incorporating real-time parameter estimation techniques such as UKF into predictive control frameworks—especially in electric vehicle applications, where precise torque control is critical outside cruising modes. The proposed strategy enhances system efficiency, robustness, and control accuracy in the presence of nonlinear and time-varying machine characteristics.

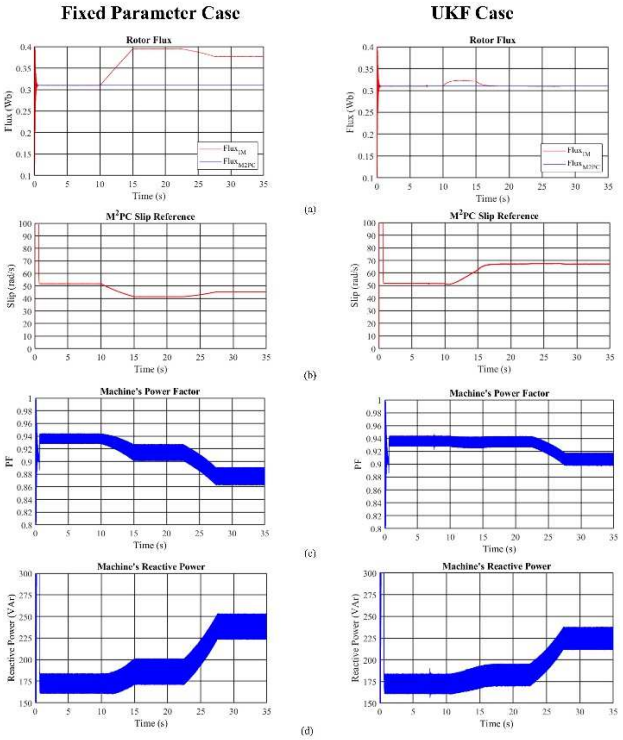

Fig. 7. Results of the designed control systems: a) Rotor flux, b) Slip, c) Power factor, d) Reactive power

REFERENCES

[1] F. Blaschke, "The Principle of Field Orientation as Applied to the New Transvector Closed Loop System for Rotating Field Machines," *Siemens Rev.*, vol. 39, pp. 217–220, 1972.

[2] I. Takahashi and T. Noguchi, "A New Quick-Response and High-

Efficiency Control Strategy of an Induction Motor," *IEEE Trans. Ind. Appl.*, vol. IA-22, no. 5, pp. 820–827, 1986, doi: 10.1109/TIA.1986.4504799.

[3] F. Wang, Z. Zhang, X. Mei, J. Rodríguez, and R. Kennel, "Advanced control strategies of induction machine: Field oriented control, direct torque control and model predictive control," *Energies*, vol. 11, no. 1, 2018, doi: 10.3390/en11010120.

[4] M. F. Elmorshedy, W. Xu, F. F. M. El-Sousy, M. R. Islam, and A. A. Ahmed, "Recent Achievements in Model Predictive Control Techniques for Industrial Motor: A Comprehensive State-of-the-Art," *IEEE Access*, vol. 9, pp. 58170–58191, 2021, doi: 10.1109/ACCESS.2021.3073020.

[5] P. Cortés, M. P. Kazmierkowski, R. M. Kennel, D. E. Quevedo, and J. Rodriguez, "Predictive control in power electronics and drives," *IEEE Trans. Ind. Electron.*, vol. 55, no. 12, pp. 4312–4324, 2008, doi: 10.1109/TIE.2008.2007480.

[6] M. Norambuena, J. Rodriguez, Z. Zhang, F. Wang, C. Garcia, and R. Kennel, "A Very Simple Strategy for High-Quality Performance of AC Machines Using Model Predictive Control," *IEEE Trans. Power Electron.*, vol. 34, no. 1, pp. 794–800, 2018, doi: 10.1109/TPEL.2018.2812833.

[7] O. Gulbudak and M. Gokdag, "Finite control set model predictive control approach of nine switch inverter-based drive systems: Design, analysis, and validation," *ISA Trans.*, vol. 110, pp. 283–304, 2021, doi: 10.1016/j.isatra.2020.10.037.

[8] T. Wu *et al.*, "Enhanced Model Predictive Control for PMSM Based on Reference Voltage Predictive Model," *IEEE J. Emerg. Sel. Top. Power Electron.*, vol. 11, no. 5, pp. 5290–5300, Oct. 2023, doi: 10.1109/JESTPE.2023.3307469.

[9] X. Gao *et al.*, "Model Predictive Control of a Modular Multilevel Converter Considering Control Input Constraints," *IEEE Trans. Power Electron.*, vol. 39, no. 1, pp. 636–648, Jan. 2024, doi: 10.1109/TPEL.2023.3318320.

[10] Q. Li, H. Li, J. Gao, and R. Kennel, "Model Predictive Control Using the Singular Perturbation Theory for Permanent-Magnet Synchronous Machines," *IEEE Trans. Power Electron.*, vol. 39, no. 3, pp. 3533–3543, Mar. 2024, doi: 10.1109/TPEL.2023.3341455.

[11] S. Vazquez, J. Rodriguez, M. Rivera, L. G. Franquelo, and M. Norambuena, "Model Predictive Control for Power Converters and Drives: Advances and Trends," *IEEE Trans. Ind. Electron.*, vol. 64, no. 2, pp. 935–947, 2017, doi: 10.1109/TIE.2016.2625238.

[12] J. Rodriguez *et al.*, "Latest Advances of Model Predictive Control in Electrical Drives - Part I: Basic Concepts and Advanced Strategies," *IEEE Trans. Power Electron.*, vol. 37, no. 4, pp. 3927–3942, Apr. 2022, doi: 10.1109/TPEL.2021.3121532.

[13] J. P. Zucuni, F. Carnielutti, H. Pinheiro, M. Norambuena, and J. Rodriguez, "Cost Function Design for Stability Assessment of Modulated Model Predictive Control," in *2020 22nd European Conference on Power Electronics and Applications, EPE 2020 ECCE Europe*, 2020, pp. 1–9, doi: 10.23919/EPE20ECCEEurope43536.2020.9215797.

[14] U. U. Korpe, M. Gokdag, M. Koç, and O. Gulbudak, "Modulated Model Predictive Torque Control for Interior Permanent Magnet Synchronous Machines," *El-Cezeri*, vol. 2022, no. 2, pp. 777–787, 2022, doi: 10.31202/ecjse.1008121.

[15] D. Xiao, K. S. Alam, M. P. Akter, S. M. S. I. Shakib, D. Zhang, and M. Rahman, "Modulated Model Predictive Control for Four-Leg Inverters with Online Duty Ratio Optimization," *IEEE Trans. Ind. Appl.*, vol. 56, no. 3, pp. 3114–3124, 2020, doi: 10.1109/TIA.2020.2971448.

[16] M. Ayala, J. Doval-Gandoy, J. Rodas, O. Gonzalez, R. Gregor, and M. Rivera, "A Novel Modulated Model Predictive Control Applied to Six-Phase Induction Motor Drives," *IEEE Trans. Ind. Electron.*, vol. 68, no. 5, pp. 3672–3682, 2021, doi: 10.1109/TIE.2020.2984425.

[17] O. Gonzalez *et al.*, "Model Predictive Current Control of Six-phase Induction Motor Drives using Virtual Vectors and Space Vector Modulation," *IEEE Trans. Power Electron.*, vol. 37, no. 7, pp. 7617–7628, 2022, doi: 10.1109/TPEL.2022.3141405.

[18] J. Andino, P. Ayala, J. Llanos-Proano, D. Naunay, W. Martinez, and D. Arcos-Aviles, "Constrained Modulated Model Predictive Control for a Three-Phase Three-Level Voltage Source Inverter," *IEEE Access*, vol. 10, pp. 10673–10687, 2022, doi: 10.1109/ACCESS.2022.3144669.

[19] M. Gokdag, "Modulated Predictive Control to Improve the Steady-State Performance of NSI-Based Electrification Systems," *Energies*, vol. 15, no. 6, 2022, doi: 10.3390/en15062043.

[20] G. Book *et al.*, "Transferring online reinforcement learning for electric motor control from simulation to real-world experiments," *IEEE Open J. Power Electron.*, vol. 2, pp. 187–201, 2021, doi: 10.1109/OJPEL.2021.3065877.

[21] A. Traue, G. Book, W. Kirchgassner, and O. Wallscheid, "Toward a Reinforcement Learning Environment Toolbox for Intelligent Electric Motor Control," *IEEE Trans. Neural Networks Learn. Syst.*, vol. 33, no. 3, pp. 919–928, Mar. 2022, doi: 10.1109/TNNLS.2020.3029573.

[22] M. Akbaba, M. Taleb, and A. Rumeli, "Improved estimation of induction machine parameters," *Electr. Power Syst. Res.*, vol. 34, no. 1, pp. 65–73, 1995, doi: 10.1016/0378-7796(95)00958-K.

[23] S. M. N. Hasan and I. Husain, "A Luenberger-sliding mode observer for online parameter estimation and adaptation in high-performance induction motor drives," *IEEE Trans. Ind. Appl.*, vol. 45, no. 2, pp. 772–781, 2009, doi: 10.1109/TIA.2009.2013602.

[24] D. Jakobeit, M. Schenke, and O. Wallscheid, "Meta-Reinforcement-Learning-Based Current Control of Permanent Magnet Synchronous Motor Drives for a Wide Range of Power Classes," *IEEE Trans. Power Electron.*, vol. 38, no. 7, pp. 8062–8074, Jul. 2023, doi: 10.1109/TPEL.2023.3256424.

[25] H. Xie, F. Wang, Y. He, J. Rodríguez, and R. Kennel, "Encoderless Parallel Predictive Torque Control for Induction Machine Using a Robust Model Reference Adaptive System," *IEEE Trans. Energy Convers.*, vol. 37, no. 1, pp. 232–242, 2022, doi: 10.1109/TEC.2021.3102305.

[26] J. Zhang, X. Zhang, Y. Yu, B. Wang, and D. Xu, "A Model Reference Adaptive System-Based Online Rotor Time Constant Estimation Method for Induction Motor Field-Weakening Control Utilizing Dot Product of Stator Voltage and Stator Current," *IEEE Trans. Transp. Electrif.*, 2023, doi: 10.1109/TTE.2023.3310517.

[27] R. Demir, "Robust stator flux and load torque estimations for induction motor drives with EKF-based observer," *Electr. Eng.*, vol. 105, no. 1, pp. 551–562, 2023, doi: 10.1007/s00202-022-01717-y.

[28] S. A. Davari *et al.*, "Extended Kalman Filter as the Prediction Model in Sensorless Predictive Control of Induction Motor," Jul. 2023, doi: 10.1109/PRECEDE57319.2023.10174332.

[29] E. Zerdali, M. Rivera, P. Zanchetta, P. Wheeler, and L. Ristic, "Encoderless Predictive Speed and Torque Control of an Induction Motor," *Proc. 22nd Int. Symp. Power Electron. Ee 2023*, 2023, doi: 10.1109/Ee59906.2023.10346148.

[30] K. Horváth and M. Kuslits, "Dynamic Performance of Estimator-based Speed Sensorless Control of Induction Machines Using Extended and Unscented Kalman Filters," *Power Electron. Drives*, vol. 3, no. 1, pp. 129–144, 2018, doi: 10.2478/pead-2018-0003.

[31] R. Yildiz, M. Barut, and E. Zerdali, "A Comprehensive Comparison of Extended and Unscented Kalman Filters for Speed-Sensorless Control Applications of Induction Motors," *IEEE Trans. Ind. Informatics*, vol. 16, no. 10, pp. 6423–6432, 2020, doi: 10.1109/TII.2020.2964876.

[32] J. K. Uhlmann, *Dynamic Map Building and Localization: New Theoretical Foundations*. University of Oxford, 1995.

[33] S. J. Julier and J. K. Uhlmann, "New extension of the Kalman filter to nonlinear systems," *Signal Process. Sens. Fusion, Target Recognit. VI*, vol. 3068, p. 182, 1997, doi: 10.1117/12.280797.

[34] S. Rigon, B. Haus, P. Mercorelli, and M. Zigliotto, "Comparison between UKF and EKF in Sensorless Synchronous Reluctance Motor Drives," *IEEE Open J. Power Electron.*, vol. 5, no. September, pp. 1562–1572, 2024, doi: 10.1109/OJPEL.2024.3469533.

[35] J. Rodriguez *et al.*, "Predictive Current Control of a Voltage Source Inverter," *IEEE Trans. Ind. Electron.*, vol. 54, no. 1, pp. 495–503, 2007, doi: 10.1109/TIE.2006.888802.

[36] M. Gokdag and O. Gulbudak, "Dual-model predictive control of two independent induction motors driven by a SiC nine-switch inverter," *Int. J. Electron.*, vol. 00, no. 00, pp. 1–19, 2021, doi: 10.1080/00207217.2021.2007545.

[37] C. Garcia, J. Rodriguez, S. Odhano, P. Zanchetta, and S. A. Davari, "Modulated Model Predictive Speed Control for PMSM Drives," in *2018 IEEE International Conference on Electrical Systems for Aircraft, Railway, Ship Propulsion and Road Vehicles and International Transportation Electrification Conference, ESARS-ITEC 2018*, 2019, no. 1, pp. 1–6, doi: 10.1109/ESARS-ITEC.2018.8607701.